

Numerical Simulations Show Potential for Strong Non-isothermal Effects During Fluid Leakage from a Geologic Disposal Reservoir for CO₂

Karsten Pruess

Earth Sciences Division, Lawrence Berkeley National Laboratory, Berkeley, CA 94720

Leakage of CO₂ from a primary disposal reservoir is presumed to occur along a fault or fracture zone, which has been modeled as a slab of porous and permeable material embedded in wall rocks of negligibly small permeability. Numerical simulations presented here include multiphase flow, boiling of liquid CO₂, transitions between supercritical and subcritical conditions, phase partitioning between CO₂ and water, and non-isothermal effects. Depressurization of rising CO₂ is found to produce strong cooling. Conductive heat transfer from the impermeable wall rocks is an important aspect of system evolution. Pressure and temperature conditions are drawn towards the critical point of CO₂ and the CO₂ saturation line. The interplay between multiphase flow in the fracture zone and heat conduction perpendicular to it may produce non-monotonic, quasi-periodic variations in thermodynamic conditions.

Introduction

The amounts of CO₂ generated by fossil-fueled power plants are enormous, approximately 30,000 tonnes per day (10 million tonnes per year) for a coal-fired plant with 1,000 MW electric output (Hitchon, 1996). Among the different concepts currently being studied for reducing atmospheric emissions of greenhouse gases, one of the more promising ones involves disposal into deep geologic formations. Containment of CO₂ in geologic structures is not expected to be perfect. Disposal of CO₂ in saline aquifers would generate plumes that over a typical life time of a power plant of 30-50 years would extend over a large area of 100 km² or more (Pruess et al., 2003). This would make it all but inevitable that caprock weaknesses such as faults or fracture zones will be encountered that provide pathways for CO₂ leakage from the primary disposal reservoir. An assessment of the feasibility of geologic disposal requires an understanding of the manner in which CO₂ may escape and ultimately be discharged at the land surface.

The behavior of CO₂ depends on the hydrogeologic properties of the pathways along which it migrates, on the thermodynamic regime encountered (temperature and pressure conditions), and on the thermophysical properties of CO₂ and resident aqueous fluids.

In a previous study, the pathway for CO₂ escape from the storage reservoir was modeled as a circular vertical channel of 3 m radius, embedded in a porous medium of lower permeability, and extending from 1000 m depth straight up to the ground surface (Pruess, 2004). In the present paper we consider migration along a 2-D planar feature that is intended to represent a generic

fault or fracture zone (Fig. 1). Our main interest is in the thermodynamic regime and the coupled fluid flow and heat transfer effects during migration of CO₂.

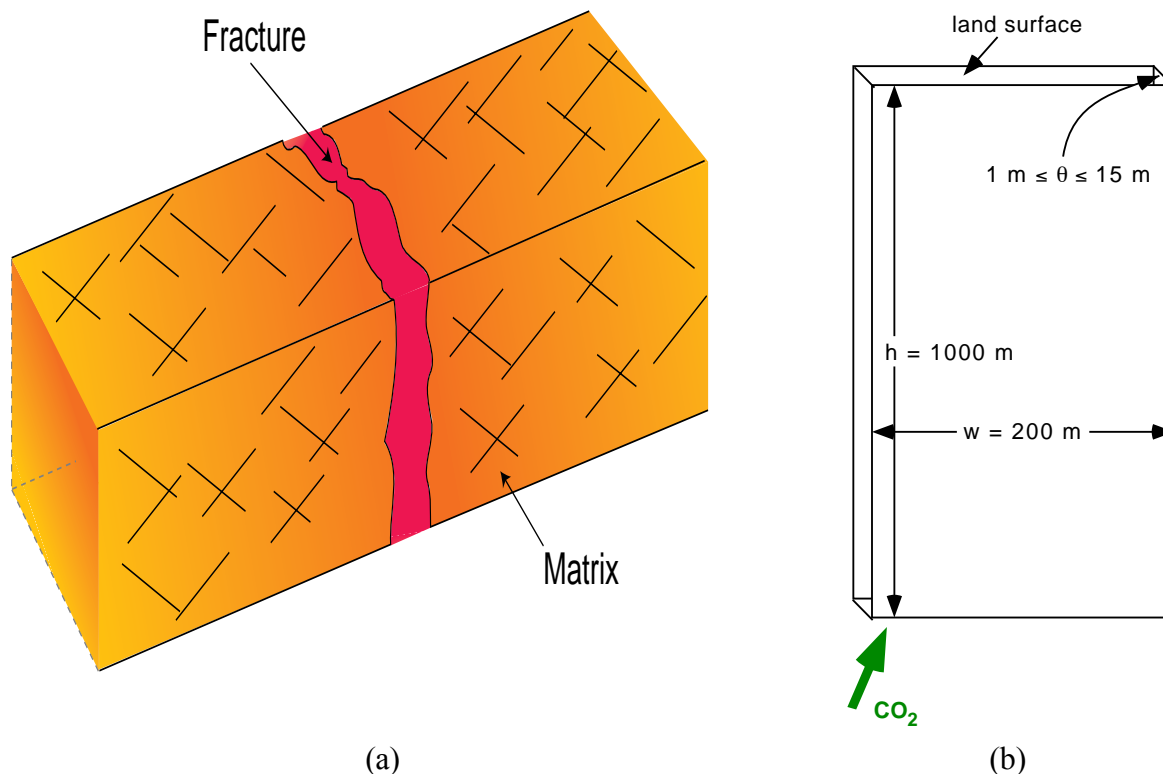


Figure 1. Simple model of a fracture zone used for modeling CO₂ escape from a geologic disposal reservoir. The conceptual model (a) involves a fault or fracture zone sandwiched between matrix rock of negligibly small permeability. The specific simulation problem considered in this paper involves a rectangular high-permeability zone of 200 m width, that is assumed to extend from a CO₂ reservoir at 1000 m depth all the way to the land surface (b). CO₂ migration was studied for different thicknesses of this zone in the range from 1 to 15 m.

Thermodynamic Issues

There is a general consensus in the technical community that CO₂ would be sequestered as a liquid or supercritical fluid (Holloway and Savage, 1993; Hitchon et al., 1999). The thermodynamic issues relevant to upflow of CO₂ from a deep storage reservoir are illustrated in Fig. 2a. The saturated vapor pressure of CO₂ as a function of temperature is shown along with two hydrostatic pressure profiles, calculated for a typical geothermal gradient of 30 °C per km, for two average land surface temperatures of 5 °C and 15 °C. Both profiles pass in the vicinity of the critical point of CO₂ ($T_{\text{crit}} = 31.04 \text{ °C}$, $P_{\text{crit}} = 73.82 \text{ bar}$), and the one for 5 °C surface temperature intersects the CO₂ saturation line. In the latter case a bubble of CO₂ that is migrating upward would undergo a phase transition from liquid to gas at a pressure of approximately 63 bars, corresponding to a depth of approximately 630 m. Leakage of CO₂ from a deeper brine

formation may induce some overpressure, which would shift the pressure profiles towards higher values. Phase change from liquid to gas is to be expected if CO₂ escapes upward at rates large enough so that not all of the leaking CO₂ dissolves in the aqueous phase. Boiling of liquid CO₂ may have large effects on leakage rates, because CO₂ density is much lower for the gaseous than for the liquid state (Fig. 2b). At subsurface (T, P) conditions, CO₂ is always less dense than the aqueous phase and thus is subject to an upward buoyancy force. A transition to gaseous conditions would greatly enhance the buoyancy forces and accelerate fluid leakage, as well as causing a rapid increase in fluid pressures at shallower horizons. This in turn could open pre-existing faults and fractures, enhancing their permeability and further increasing leakage rates.

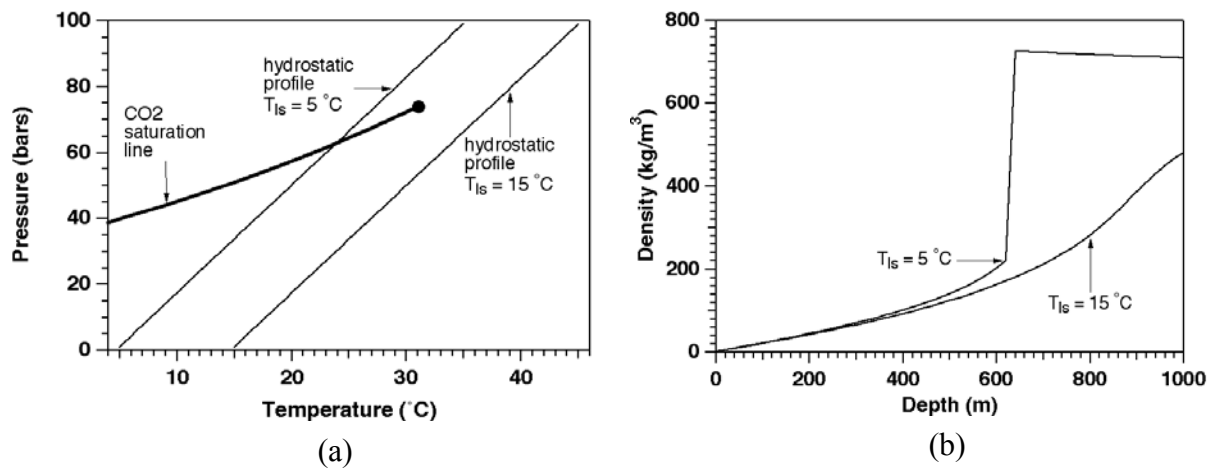


Figure 2. (a) CO₂ saturation line and hydrostatic pressure-temperature profiles for typical continental crust; (b) density of CO₂ vs. depth for the two hydrostatic profiles shown in Fig. 2a.

The specific enthalpy of CO₂ increases upon decompression, even if no phase change occurs (as e.g. along the $T_{ls} = 15^\circ\text{C}$ line shown in Fig. 2a), so that CO₂ migrating upward towards lower pressures would tend to undergo cooling as it expands. Inside a porous medium, the temperature decline is buffered by heat transfer from the solids. Heat transfer between rocks and fluids occurs locally on the pore scale, and also over larger distances by means of heat conduction from the low-permeability country rock towards the CO₂ pathway. Additional thermal effects occur when advancing CO₂ partially dissolves in aqueous fluids, giving rise to a small temperature increase from heat-of-dissolution effects.

Approach

The fracture zone considered as a leakage path for CO₂ in this paper is shown in Fig. 1, and is modeled as a homogeneous porous medium sandwiched between impermeable walls. Permeability of the fracture zone is assumed as 10^{-13} m^2 , and porosity is taken as 0.35. Initial conditions are

prepared by allowing a water-saturated system to run to steady state corresponding to land surface conditions of $T_{ls} = 15\text{ }^{\circ}\text{C}$, $P_{ls} = 1.013 \times 10^5\text{ Pa}$, and a geothermal gradient of $30\text{ }^{\circ}\text{C/km}$ (see Fig. 2a). Boundary conditions at 1000 m depth are a temperature of $45\text{ }^{\circ}\text{C}$, and a hydrostatic pressure of $98.84 \times 10^5\text{ Pa}$. In the present study we do not specify the nature of the CO_2 storage reservoir, nor do we model the temporal and spatial variability with which CO_2 may escape from primary storage. Instead, leakage is initiated by applying CO_2 at a slight overpressure of $99.76 \times 10^5\text{ Pa}$ over a width of 6 m at the bottom left hand side of the fracture zone. Boundary conditions at the top are maintained unchanged throughout the simulation. Lateral boundaries are "no flow." The walls bounding the fracture zone are assumed impervious to fluids but are participating in conductive heat exchange with the fluids in the fracture.

All simulations were performed with the general-purpose code TOUGH2 (Pruess et al., 1999), using a newly developed fluid property module that includes all seven possible phase combinations in the three-phase system aqueous - liquid CO_2 - gaseous CO_2 , as well as transitions between super- and sub-critical fluid (Pruess, 2004). Thermophysical properties of CO_2 are represented, within experimental accuracy, by the correlations of Altunin (Altunin, 1975; Pruess and García, 2002). These were extensively cross-checked against experimental data and alternative PVT formulations, such as Span and Wagner (1996), and were found to be very accurate (García, 2003). Our main reason for using Altunin's correlations is that a computer program implementing them was conveniently made available to us, thanks to Victor Malkovsky of IGEM, Moscow.

For numerical simulation, the fault zone is discretized into rectangular blocks, with vertical grid spacing of 20 m and horizontal grid spacing varying from 2 m at the left boundary, where CO_2 is introduced (Fig. 1b), to 10 m at the right boundary. Although fluid flow is confined to the two-dimensional permeable medium within the fault zone, heat exchange with the wall rocks is a very important aspect of system behavior. The wall rocks are not explicitly included in the definition domain of the model; instead they are modeled with the semi-analytical method of Vinsome and Westerveld (1980), thereby reducing the dimensionality of the problem to 2-D. The wall rocks are conceptualized as semi-infinite, impermeable and purely conductive domains, and the temperature profile in the direction perpendicular to the fault zone is represented by means of a simple trial function, consisting of an exponential tail modified by a low-order polynomial.

$$T(x,t) - T_i = \left(T_f - T_i + px + qx^2 \right) \exp(-x / d) \quad (1)$$

In the context of a finite-difference simulation of nonisothermal flow, each grid block in the fault zone will have an associated temperature profile in the adjacent impermeable rock as given by Eq. (1). Here x is the penetration depth into the conductive domain, t is time, T_i is initial temperature in the wall rock (assumed uniform in the direction perpendicular to the fault zone, but will in our case be different for grid blocks at different elevations, due to the geothermal gradient), T_f is the time-varying temperature at the wall rock boundary, p and q are time-varying fit parameters, and d is the penetration depth for heat conduction, given by

$$d = \sqrt{\Theta t}/2 \quad (2)$$

where $\Theta = \lambda/\rho C$ is the thermal diffusivity, λ the thermal conductivity, ρ the density of the medium, and C the specific heat. For the parameters $\lambda = 2.51 \text{ W/m } ^\circ\text{C}$, $\rho = 2600 \text{ kg/m}^3$, and $C = 920 \text{ J/kg}$ used here, we have $\Theta = 1.05 \times 10^{-6} \text{ m}^2/\text{s}$. The coefficients p and q are different for different grid blocks and are determined concurrently with the flow simulation from the following physical constraints: (1) temperatures throughout the conductive domain must satisfy a heat conduction (diffusion) equation, and (2) cumulative heat flow across the boundary must equal the change of thermal energy in the conductive domain. In the wall rocks, only heat conduction perpendicular to the fault zone is taken into account. Numerous test calculations have shown the Vinsome-Westerveld technique to provide excellent accuracy for conductive heat exchange, even under conditions of non-monotonic temperature variations in the fluid flow domain (Vinsome and Westerveld, 1980; Pruess and Wu, 1993).

By varying the thickness θ of the fracture zone (Fig. 1b) the strength of heat transfer relative to fluid flow can be varied in a systematic manner. If heat transfer across the fault zone walls is neglected, system evolution is independent of thickness, and CO_2 flow rate at any given time is proportional to the fault zone thickness. If heat conduction across the fault zone boundaries is accounted for, the perturbation of the ambient temperature profile will be smaller for a smaller fault zone thickness, as a smaller rate of CO_2 flow means a smaller rate of heat transfer from cooling during decompression. The rate of heat transfer to the flowing CO_2 will tend to zero for $\theta \rightarrow 0$, corresponding to the limiting case of keeping all temperatures unchanged at their initial values. In the opposite limit $\theta \rightarrow \infty$, heat transfer per unit rate of fluid flow will tend to zero, approaching the limit of no conductive heat transfer across the fault zone walls. Of course, as fault zone thickness gets large, thermodynamic conditions perpendicular to the walls will no longer be uniform, and the spatial variability of thermodynamic conditions in the fault zone as a function of distance from the wall rocks should be resolved through 3-D gridding. Our simulations use 2-D gridding only, with no spatial resolution perpendicular to the walls, and in that case the limit $\theta \rightarrow \infty$ will strictly

correspond to a situation of no heat transfer across the walls. We have performed simulations for fault zone thicknesses in the range $1 \text{ m} \leq \theta \leq 15 \text{ m}$, and have also simulated the limiting cases corresponding to $\theta \rightarrow 0$ and $\theta \rightarrow \infty$. In the absence of heat transfer effects all these cases would produce identical flow behavior, with flow rates strictly proportional to fault zone thickness θ . Any observed differences in system behavior for different fault zone thickness are entirely due to heat transfer effects, allowing a clear appraisal of the nature and importance of such effects.

As will be seen below, there is a tendency for thermodynamic conditions to be drawn towards the critical point during the system evolution, and to remain very close to the CO₂ saturation line for extended periods of time, in some cases undergoing frequent changes between all gas or all liquid conditions. These features make the calculation quite challenging, requiring special techniques to avoid time steps being reduced to impractical levels. Salinity effects were neglected.

Results

The CO₂ entering the column partially dissolves in the aqueous phase, but most of it forms a separate supercritical phase. Cross sections of CO₂ plumes for the case of a 15 m thick fracture zone are shown in Fig. 3 at two different times. As the CO₂ rises a three-phase zone forms (aqueous - liquid CO₂ - gaseous CO₂) which initially is thin and of limited areal extent. Fluid mobility is reduced from interference between the three phases (relative permeability effects). This tends to divert upflowing CO₂ laterally within the fault zone, broadening the three-phase zone. Continuing heat loss resulting from boiling also causes this zone to become thicker with time and to migrate towards shallower elevations. Temperatures attain a local minimum at the top of the three-phase zone, where boiling rates are largest, and over time decrease to low values, approaching the freezing point of water (Fig. 4). Our simulator currently has no provisions to treat solid ice, but there is little doubt that for the conditions investigated in this simulation, water ice and hydrate phases would form at later time. Discharge of CO₂ at the land surface begins after approximately 6 years, first by exsolution of dissolved CO₂ from water that is flowing out at the top, and followed within a few months by a free CO₂-rich gas phase reaching the top boundary of the fracture zone. Fig. 4 also shows that at early time there is a temperature increase of approximately 2-3 °C, which is due to heat-of-dissolution effects.

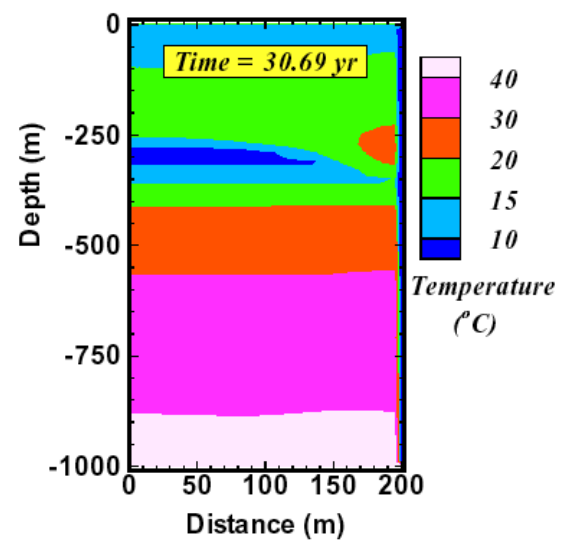
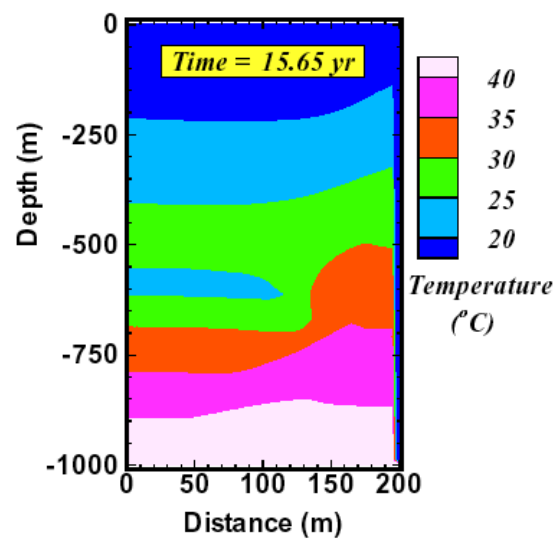
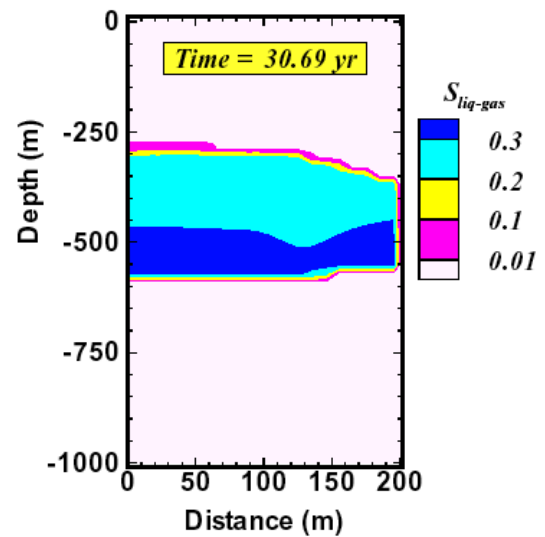
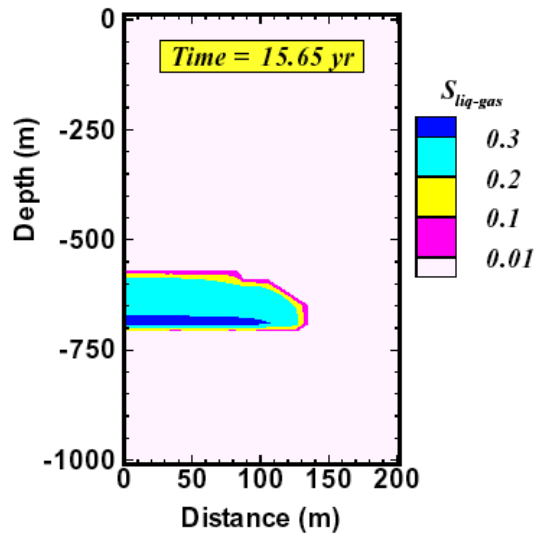
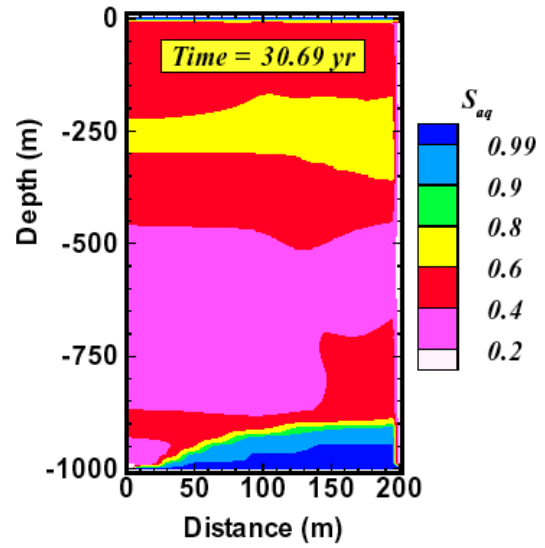
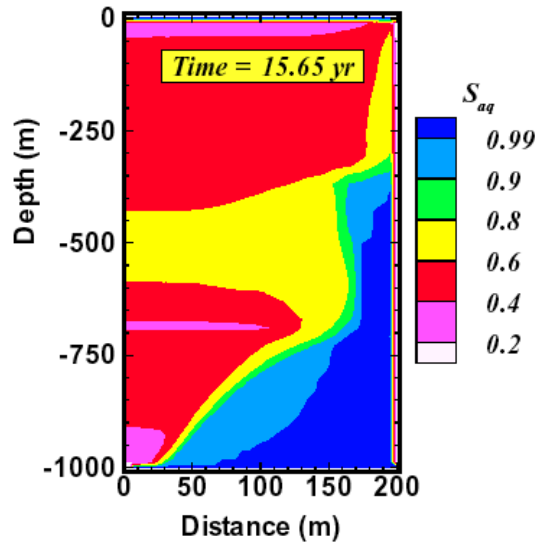


Figure 3. Snapshots of system evolution at two different times, including CO₂ plumes (top), extent of three-phase zone (middle), and temperatures (bottom). The parameter $S_{\text{liq-gas}}$ is defined as $\sqrt{S_{\text{liq}} \cdot S_{\text{gas}}}$, which is non-zero only for three-phase conditions.

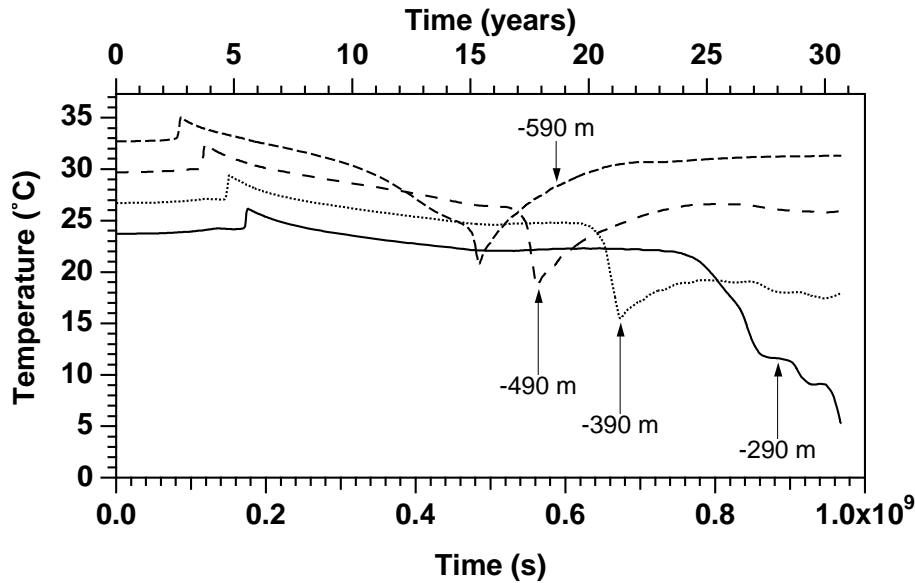


Figure 4. Temperatures at four different elevations in the leftmost column of grid blocks for a fault zone of 15 m thickness.

It is instructive to plot thermodynamic conditions in a temperature-pressure diagram. Fig. 5 shows such a diagram for the leftmost column of grid blocks above the CO₂ injection region at different times. Initial conditions are represented by the line labeled "hydrostatic profile." It is seen that after 6.07 yr the CO₂ injection has caused some temperature decline in the high (T, P)-region, at the bottom of the fracture zone. The underlying mechanism is cooling from expansion of CO₂. At the lowest pressures (shallow depths) temperatures have increased due to heat-of-dissolution effects. After a three-phase zone has formed, thermodynamic conditions track the CO₂ saturation line (15.65 and 30.69 yr in Fig. 5).

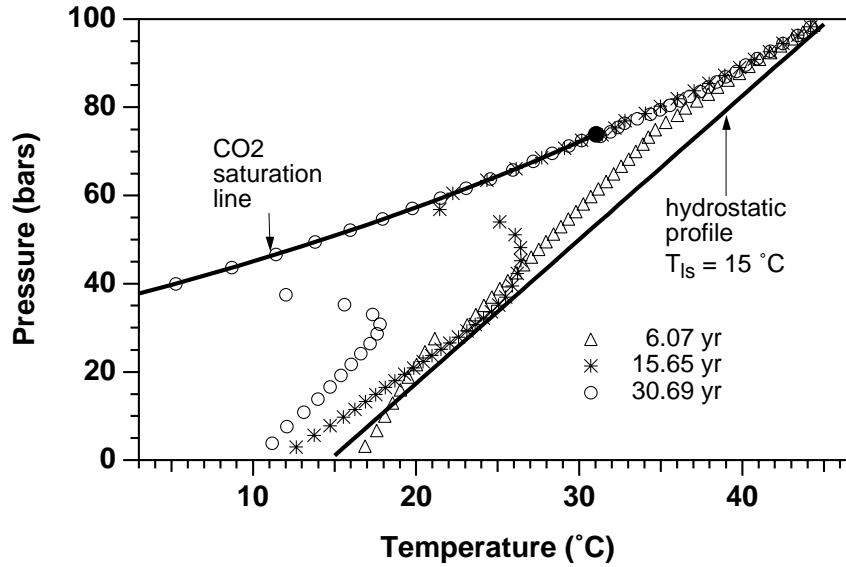


Figure 5. Pressure-temperature profiles in the leftmost column of grid blocks for a fault zone of 15 m thickness at different times.

Figs. 6 and 7 compare simulated temperature and pressure conditions in the leftmost column of grid blocks for fracture zones of different thickness after 30.69 years of simulation time. Cooling effects from expansion and boiling of liquid CO₂ are stronger for larger thickness of the fracture zone, as expected (Fig. 6a). For thicker fracture zones we obtain weaker pressure gradients at depth, beneath the three-phase zone (Fig. 6b). This indicates that leakage rates will increase less than linearly with fracture zone thickness, due to lower temperatures and larger CO₂ densities. Fig. 7 shows that the thickness of 3-phase aqueous-liquid-gas zones (extent of pressure interval along the CO₂ saturation line) at a given time will be larger for a thicker fracture zone. A simulation for a very thin fracture zone produced no 3-phase zone at all, while in the limit of a very thick fracture zone, corresponding to negligible heat transfer from the wall rocks, the 3-phase zone grows rapidly towards shallower elevations. The simulation without lateral heat transfer stopped after 24.3 yr when temperatures at the top had declined to 2.75 °C, which is the lower temperature limit of our fluid property description.

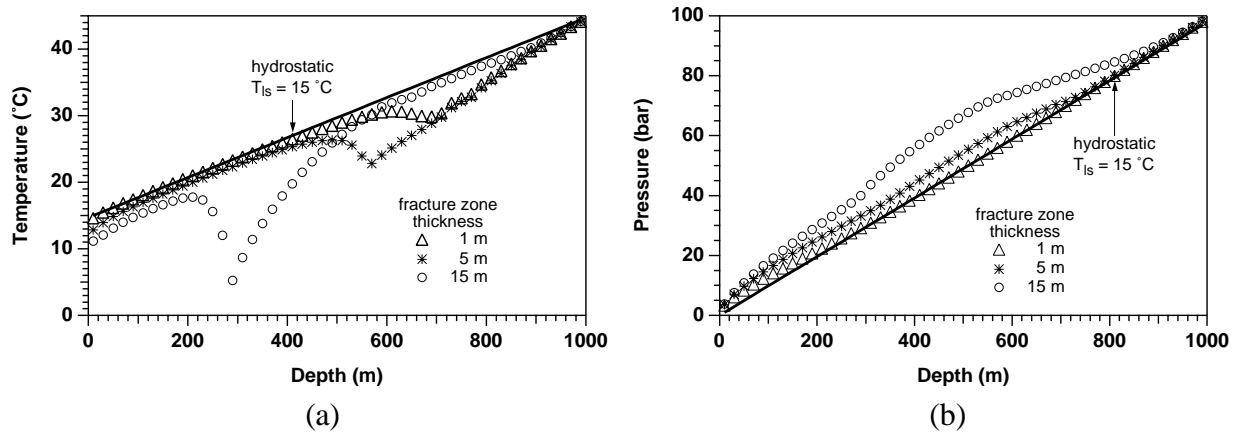


Figure 6. Temperature and pressure conditions in the leftmost column of grid blocks after 30.69 yr for fracture zones of different thickness.

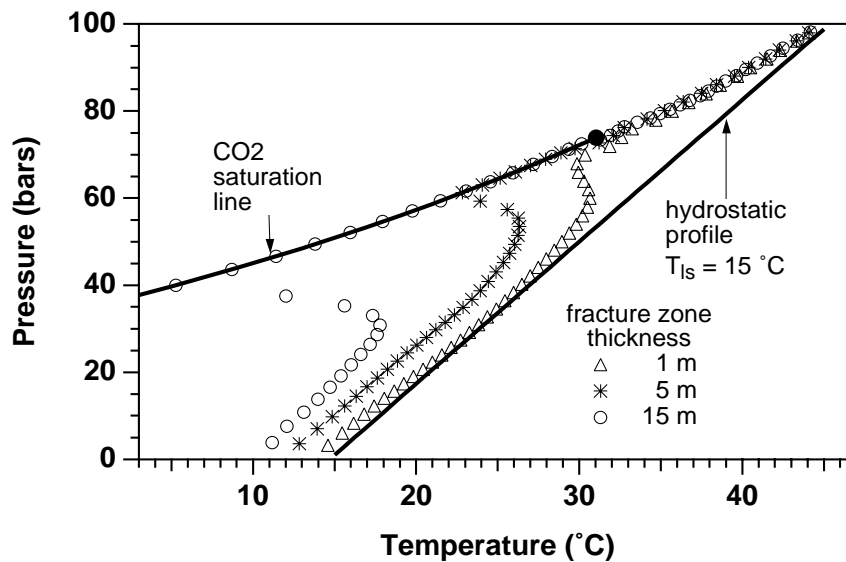


Figure 7. Pressure-temperature profiles in the leftmost column of grid blocks for fault zones of different thickness after 30.69 yr.

In some cases we observe non-monotonic variations of temperatures, pressures, and CO₂ flow rates over time. As an example, Fig. 8 shows temperatures at different elevations in the leftmost column of grid blocks for the 1 m thick fracture zone, and Fig. 9 shows total rate of CO₂ discharge at the land surface, along with the total volume of the flow system that is in 3-phase conditions. There is an anticorrelation between CO₂ flow rates and the magnitude of 3-phase volumes, showing the suppression of flow due to phase interference in the 3-phase zone. The non-monotonic variations arise from the coupling and interplay between multiphase flow in the fracture zone, and conductive heat transfer in the wall rocks (Pruess, paper in preparation).

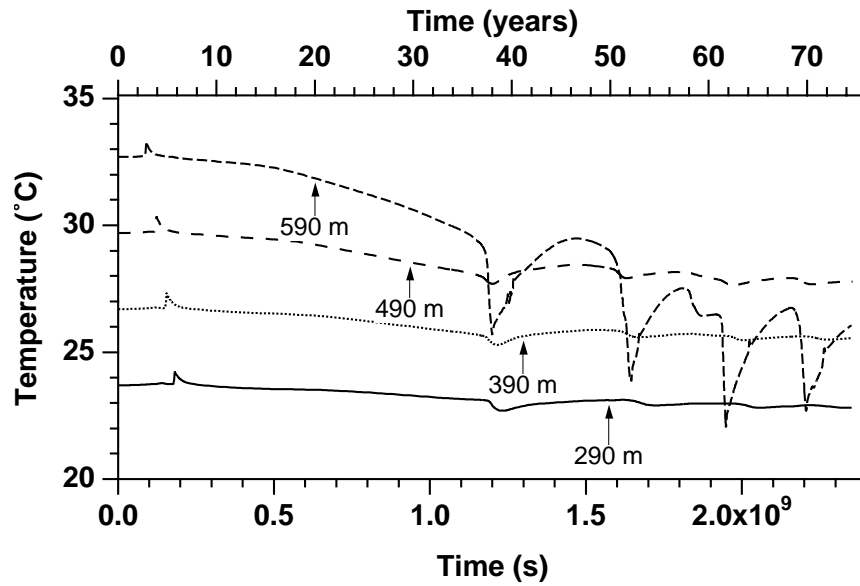


Figure 8. Temperatures at four different elevations in the leftmost column of grid blocks for a fault zone of 1 m thickness.

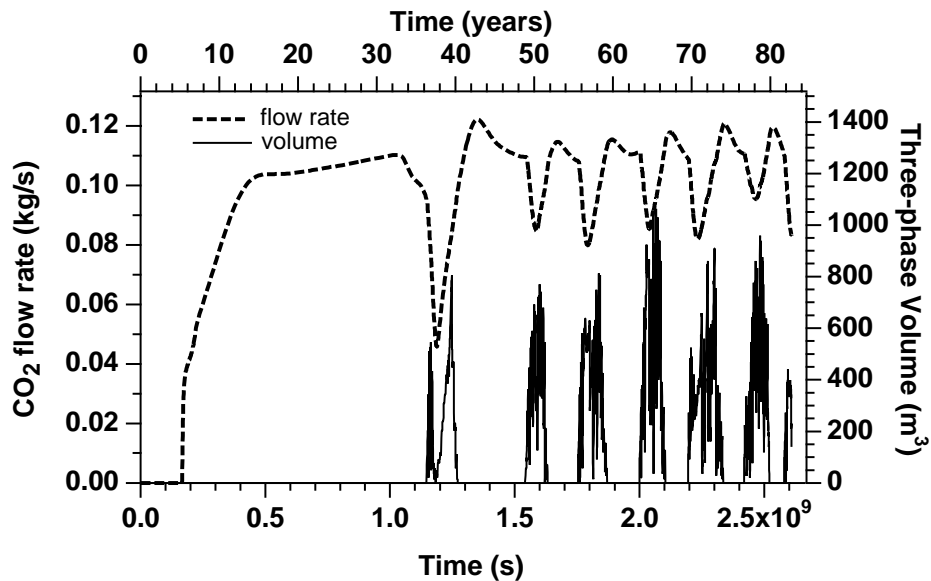


Figure 9. CO₂ flow rate across the land surface and total volume with 3-phase conditions for a fault zone of 1 m thickness.

Concluding Remarks

CO₂ migration behavior in a fault zone depends on relative rates of fluid flow and heat transfer. Simulation results presented above and additional results not shown here demonstrate the following.

- Upward migration of CO₂ along a fracture zone is strongly affected by heat transfer effects. Limited cooling occurs from expansion, while much stronger cooling takes place when liquid CO₂ boils into gas. CO₂ dissolution in the aqueous phase causes minor temperature increases.
- CO₂ migration to depths shallower than about 750 m may generate a three-phase system (aqueous - liquid CO₂ - gaseous CO₂), even if the initial hydrostatic-geothermal profile does not intersect the CO₂ saturation line.
- There is a strong tendency for thermodynamic conditions to be drawn towards the critical point of CO₂ ($T_{\text{crit}} = 31.04\text{ }^{\circ}\text{C}$, $P_{\text{crit}} = 73.82\text{ bar}$), and to remain close to the CO₂ saturation line. This gives rise to severely non-linear behavior and makes numerical simulations of leakage processes very challenging.
- The tendency towards development of three-phase zones increases with increasing thickness of the fracture zone. Increasing the permeability of the fault zone while keeping its thickness unchanged will also enhance development of three-phase zones, as it will increase the rate of CO₂ discharge relative to available conductive heat supply. When CO₂ migrates through thin fracture zones, three-phase zones may not form at all or may form and dissolve in a transient manner.
- Fluid mobility is reduced in three-phase zones, due to interference between the phases. This impedes upflow, diverting CO₂ sideways and making these zones areally more extensive.
- Continued heat loss in boiling causes temperatures to decline over time, so that three-phase zones tend to grow in thickness and advance towards shallower depths. Depending on the fracture zone thickness and permeability (CO₂ discharge rate), temperatures may reach the freezing point of water, and water ice and hydrate phases may form.
- The interplay between multiphase flow effects, phase change, and heat transfer may give rise to non-monotonic flow and temperature behavior.

Acknowledgement

Thanks are due to Christine Doughty and Pat Dobson for a careful review and suggestions for improvements. This work was supported by the Director, Office of Science, Office of Basic Energy Science of the U.S. Department of Energy under Contract No. DE-AC03-76SF00098.

References

- Altunin, V.V. *Thermophysical Properties of Carbon Dioxide*, Publishing House of Standards, 551 pp., Moscow, 1975 (in Russian).
- García, J.E. Fluid Dynamics of Carbon Dioxide Disposal Into Saline Aquifers, PhD dissertation, U. of California at Berkeley, Berkeley, California, December 2003.

- Hitchon, B. (ed.). *Aquifer Disposal of Carbon Dioxide*, Geoscience Publishing, Ltd., Sherwood Park, Alberta, Canada, 1996.
- Hitchon, B., W.D. Gunter, T. Gentzis and R.T. Bailey. Sedimentary Basins and Greenhouse Gases: A Serendipitous Association, *Energy Convers. Mgmt.*, Vol. 40, pp. 825 - 843, 1999.
- Holloway, S. and D. Savage. The Potential for Aquifer Disposal of Carbon Dioxide in the U.K., *Energy Convers. Mgmt.*, Vol. 34, No. 9-11, pp. 925 - 932, 1993.
- Pruess, K. Numerical Simulation of CO₂ Leakage from a Geologic Disposal Reservoir, Including Transitions from Super- to Sub-Critical Conditions, and Boiling of Liquid CO₂, *Soc. Pet. Eng. J.*, pp. 237 - 248, June 2004.
- Pruess, K. and J. García. Multiphase Flow Dynamics During CO₂ Injection into Saline Aquifers, *Environmental Geology*, Vol. 42, pp. 282 - 295, 2002.
- Pruess, K., C. Oldenburg and G. Moridis. TOUGH2 User's Guide, Version 2.0, Lawrence Berkeley National Laboratory Report LBNL-43134, Berkeley, CA, November 1999.
- Pruess, K. and Y. S. Wu. A New Semianalytical Method for Numerical Simulation of Fluid and Heat Flow in Fractured Reservoirs, *SPE Advanced Technology Series*, Vol. 1, No. 2, pp. 63-72, 1993.
- Pruess, K., T. Xu, J. Apps and J. García. Numerical Modeling of Aquifer Disposal of CO₂, Paper SPE-83695, *SPE Journal*, pp. 49 - 60, 2003.
- Span, R. and W. Wagner. A New Equation of State for Carbon Dioxide Covering the Fluid Region from the Triple-Point Temperature to 1100 K at Pressures up to 800 MPa, *J. Phys. Chem. Ref. Data*, Vol. 25, No. 6, 1509, 1996.
- Vinsome, P.K.W. and J. Westerveld. A Simple Method for Predicting Cap and Base Rock Heat Losses in Thermal Reservoir Simulators, *J. Canadian Pet. Tech.*, 19 (3), 87-90, July-September 1980.